LAWRENCE
LIVERMORE
NATIONAL
LABORATORY

LLNL-JRNL-516095

Testing Event Discrimination over Broad Regions using the Historical Borovoye Observatory Explosion Dataset

M. E. Pasyanos, S. R. Ford , W. R. Walter

November 23, 2011

Pure and Applied Geophysics

Disclaimer

Testing Event Discrimination over Broad Regions using the Historical Borovoye Observatory Explosion Dataset

Michael E. Pasyanos, Sean R. Ford, William R. Walter
Lawrence Livermore National Laboratory

Abstract

We test the performance of high-frequency regional P/S discriminants to differentiate between earthquakes and explosions at test sites and over broad regions using a historical dataset of explosions recorded at the Borovoye observatory in Kazakhstan. We compare these explosions to modern recordings of earthquakes at the same location. We then evaluate the separation of the two types of events using the raw measurements and those where the amplitudes are corrected for 1-D and 2-D attenuation structure. We find that high-frequency P/S amplitudes can reliably identify earthquakes and explosions and that the discriminant is applicable over broad regions as long as propagation effects are properly accounted for. Lateral attenuation corrections provide the largest improvement in the 2-4 Hz band, the use of which may allow us to examine smaller, distant events that have lower signal-to-noise at higher frequencies. We also find variations in P/S ratios among the three main nuclear testing locations within the Semipalatinsk Test Site which, due to their nearly identical paths to BRVK, must be a function of differing geology and emplacement conditions.

Introduction

High-frequency regional P/S ratios are an effective discriminant between closely-spaced earthquakes and explosions (e.g. Walter et al., 1995; Taylor, 1996; Hartse et al., 1997; Kim et al., 1997; Rodgers and Walter, 2002; Taylor et al., 2002; Bottone et al., 2002; Walter et al., 2007). The application of this discriminant to broad regions, however, has been hampered by large variations in the amplitudes of phases due to propagation effects in the crust and upper mantle. Attenuation models, which can account for much of the observed variability of regional phase amplitudes, have been shown to improve earthquake-explosion discrimination using these phases (e.g. Pasyanos and Walter, 2009; Phillips et al., 2009), at least in limited areas. While regional high-frequency data has become more widely available in recent years, evaluating the broad area impact of these models is challenging, due to the fact that most nuclear explosions were conducted only at designated test sites and that the number of nuclear tests has diminished markedly since most nations signed the 1996 Comprehensive nuclear-Test-Ban Treaty (CTBT).

The newly available Deglitched Borovoye Archive Data (Baker et al., 2009) allows us to test regional discriminants, and improvements to them, over a broad region of Central Asia. This dataset is an archive of digital seismograms derived from regional waveforms recorded at the Borovoye Observatory, northern Kazakhstan, over a thirty-year period beginning in 1966 (Richards et al., 1992). While seismograms from the observatory have been available to Western scientists since 2001 (Kim et al., 2001), the data contained a large number of glitches and did not include instrument responses for a significant

number of events, rendering it unusable for absolute amplitude studies. A joint effort by scientists at Lamont-Doherty Earth Observatory (LDEO) of Columbia University and Los Alamos National Laboratory (LANL) on deglitching the data and determining instrument responses (Kim and Ekstrom, 1996) has been completed, and the data made available to outside researchers.

The Borovoye dataset is very useful for testing discriminants using regional P/S ratios. Not only has this station recorded dozens of nuclear explosions at the Semipalatinsk Test Site (STS), approximately 700 km away, it has also recorded several Soviet Peaceful Nuclear Explosions (PNEs) which were widely dispersed throughout the territories of the Former Soviet Union and are distributed about the recording station. Many explosions in this Borovoye dataset were still unusable due to dropouts, clipped waveforms, or poor signal-to-noise ratio. Still, the number and distribution of the events are sufficient to provide a good test of our ability to use the discriminant over broad regions.

In this paper, we will review the methods we have been using to make regional amplitude measurements, form discriminants, and tomographically invert for an attenuation model. We will then apply these methods to recordings made at the Borovoye observatory to test regional earthquake-explosion discrimination over broad areas.

Method

The basic dataset for both the discriminant and the attenuation tomography are the amplitude measurements of regional phases (Pn, Pg, Sn, Lg) in a series of narrow passbands. Arrival times of all the regional phases were made by hand, as structural complexity prohibits us from reliably using group velocity windows. Amplitude measurements from explosions were made on the three systems (KOD, SS, TSG) in the Deglitched Borovoye Archive Data (Baker et al., 2009). As only explosions were available in the archive, amplitudes for earthquakes were made on the modern instrument at BRVK. BRVK is part of the IDA (International Deployment of Accelerometers) component of the Global Seismographic Network (GSN) and the data is available from IRIS (Incorporated Research Institutes for Seismology) at www.iris.gov. The modern instrument is located at the same physical site as the historic stations. Although it might seem that we are mixing apples and oranges by comparing amplitudes from explosions on the archived data with amplitudes from earthquakes from the modern instrument, all measurements are made in absolute amplitudes (displacement) and should not matter, as long as the instrument responses are correct. We have found no issue with the responses.

The regional P/S discriminant can be manifested in a number of forms, but usually as Pn/Lg, Pg/Lg, or Pn/Sn. For propagation through the platforms (e.g. Kazakh Platform, West Siberian Platform) of Central Asia, Pn/Sn appears to be the best combination of phases to use, as both Pn and Sn propagate efficiently in the upper mantle out to long distances, where most of the natural seismicity occurs. Another consideration is the frequency band where the amplitude measurements are made. Higher-frequencies are generally thought to discriminate better (e.g. Walter et al., 1995; Hartse et al., 1997), but

both lower signal and higher noise conspire to produce poor signal-to-noise ratios at these frequencies for a number of events.

We initially considered amplitude ratios in passbands of 0.5-1, 1-2, 2-4, 4-6, 6-8, and 8-10 Hz, although we found that we had significantly fewer amplitude measurements passing signal-to-noise in the 0.5-1 Hz passband and above 6 Hz. Also, for the same reasons, the attenuation tomography has markedly poorer coverage in this relatively aseismic region above 6 Hz. We will therefore be mainly considering the 2-4 and 4-6 Hz passbands.

The regional phase amplitudes are also used in an attenuation tomography. LLNL has developed an amplitude inversion method that utilizes an MDAC (Magnitude Distance Amplitude Correction) source model (Walter and Taylor, 2001) and has been applied in a simultaneous multi-phase (Pn, Pg, Sn, Lg) amplitude tomography (Pasyanos et al., 2009). Inverting all phases simultaneously allows us to determine consistent attenuation, site, and source terms for all phases, and eliminates non-physical inconsistencies among them. Although we are concentrating on the Pn and Sn phases, which are primarily sensitive to the attenuation structure of the upper mantle, these phases have crustal legs and the amplitudes of the Pg and Lg phases provide additional constraints on the crustal attenuation structure.

From the 2009 study, we have expanded our tomography from the Middle East to cover more of Eurasia, including Central Asia. A map (**Figure 1a**) shows the dominance of structural platforms (e.g. Kazakh Platform, West Siberian Platform, Russian Platform) across the region. Most seismicity occurs to the south, although only the events to the south and southeast are at regional distances from station BRVK. **Figure 1b** shows a map of Pn paths. Note the excellent coverage in the south where seismicity is high, and much sparser coverage in the north where stations like BRVK and ARU (Arti, Russia) primarily observe events to the south. Because of the poor prediction of their S-wave amplitudes, known explosions like the PNEs are not currently used in the tomography, although the future incorporation of them (through the use of an explosion S-wave model) might significantly improve our coverage of this region. **Figure 1c** shows a map of upper mantle Qp, which is what the Pn paths shown in **Figure 1b** are primarily sensitive to. We find high Q (low attenuation) in the platforms to the north, with lower Q (high attenuation) in the tectonic regions to the south. We find very low Q in the Tian Shan, but high Q under the Tarim Basin. The Ural Mountains do not have sufficient coverage to be observed relative to the adjacent platforms. **Figure 1d** shows the path-averaged attenuation for Pn from BRVK to points in our model. Because the Q near BRVK is high, paths to Borovoye from the whole region tend to have high path-averaged Qs, although there is an important gradient from high Q to moderate Q for events to the southwest.

Regional Discrimination

The simplest discriminant (referred to here as “raw”) is to take the ratios between the P and S wave amplitudes. Normally, the result is plotted on the log scale, where

earthquakes tend to have low or negative values (large S-wave amplitude relative to P), while explosions have high values (small relative S-wave amplitudes). **Figure 2** shows maps of presumed earthquakes (circles) and explosions (stars) recorded at station BRVK in the 2-4 Hz (**Figure 2a**) and 4-6 Hz (**Figure 2b**) passbands. One of the first things to see is that the vast majority of earthquakes recorded at regional distances (approximately between the two concentric circles on the maps) from BRVK occur to the southeast of the station. Events occurring outside of this region may be due to man-made activity rather than natural seismicity, a point we will return to later. Notice as well the large cluster of explosions at the STS, as well as the Meridian PNEs to the south, the Batholith-2 PNE to the southwest, and the Hellum-1 (sometimes referred to as Helium-1) PNE to the northwest (**Table 1**).

Very clearly, based on the raw amplitudes, the discriminant does not work well, having negative ratios in the 2-4 Hz passband for the STS explosions and high positive values for many earthquakes, especially at far regional distances. In the 4-6 Hz passband, the explosions have higher P/S ratios, but there is great overlap in the populations. At the higher frequency, we also have fewer earthquakes (78) that pass the signal-to-noise criteria, as compared to the 2-4 Hz band (112 earthquakes). When plotted as a function of distance (**Figure 2c,d**), it is clear that strong trends with distance do not allow the raw discriminant to be effectively used over broad areas.

Some of the trends shown in **Figure 2c,d** are due to 1-D variations such as different Q and, perhaps, geometrical spreading of the Pn and Sn phases. If so, they can be modeled and the effects removed. We do this by modeling the earthquakes for a Magnitude Distance Amplitude Correction (MDAC) which takes into account both 1-D variations in propagation (attenuation and geometrical spreading) and magnitude, which affects the corner frequency of an event. We assume the geometrical spreading of Pn and Sn are the same, and a power-law frequency-dependent Q is modeled as:

$$Q(f) = Q_o f^{\eta} \qquad (1)$$

where Q_o is the attenuation parameter Q at 1 Hz, η its power-law frequency-dependence, and f is at the quarter frequency of the high and low passbands (e.g. 2.5 Hz for 2-4 Hz). For Pn and Sn, we find Q_o=370, η=0.38 for Pn and Q_o=450, η=0.45 for Sn. We then perform a grid search of all earthquake amplitudes recorded at BRVK for Q_o, η, and site corrections. This results in Q=523 and Q=619 for Pn and Sn, respectively, in the 2-4 Hz band and Q=653 and Q=806 for Pn and Sn in the 4-6 Hz band.

The discriminant can then be improved by taking the observed amplitudes and correcting them for the amplitudes of an earthquake (of that size, at that location) as

$$\text{discriminant} = \log[A^P/A^S] - \log[A^P{}_o/A^S{}_o] \qquad (2)$$

where the o indicates predicted amplitudes. The predicted amplitudes will be a product of four terms (source, geometrical spreading, attenuation, and site), all defined according

to the MDAC model. By normalizing the discriminant in this way, the earthquakes should scatter around the zero value.

Results are shown in **Figure 3**. Large trends are removed, especially in the 2-4 Hz passband, but some trends in the earthquakes still remain. As expected the earthquake population scatters about the ordinate of zero, and the explosions now have more positive values than the earthquakes. As a result, the discriminant improves significantly over the raw ratios, better separating the two populations. There are also some obvious and significant outliers, both for a few events labeled as earthquakes, as well as the Hellum-1 explosion that we take up in the discussion section below.

It appears that a 1-D correction can allow the discriminant to work over the full regional distance range. Can we use information on the lateral attenuation structure of the earth to further improve our discriminant? We test this by replacing the predicted amplitudes described in equation (2) with amplitudes where the attenuation term depends on the path. The results are shown in **Figure 4**. Most of the trends in the earthquake population that still existed using the 1-D model are removed and, with the exception of the same outlier events, separate cleanly into earthquake and explosion populations. As expected, the anomaly of the explosion Hellum-1 does not change. It should also be noted that path coverage north of station BRVK is poor (**Figure 1b**) and the tomographic model is essentially 1-D in this region (**Figure 1c**).

We look at the events in a slightly different way in **Figure 5**. Here we plot the discriminant as a function of magnitude, rather than distance, for the two bands we considered. There do not seem to be any trends in the data with event size. Here, we can see a larger separation between the two populations at 4-6 Hz, but the scatter of each population is also higher.

We can quantify the separation of the earthquake and explosion populations by using the Mahalanobis distance (e.g. Hartse et al., 1998), a measure of separation of the means divided by a sum of the variances.

$$\Delta^2 = \frac{\left(\bar{\mu}_x - \bar{\mu}_q\right)^2}{\left(\sigma_x^2 + \sigma_q^2\right)} \qquad (3)$$

where $\bar{\mu}$ and σ are the mean and standard deviation and subscripts x and q refer to explosions and earthquakes. A larger Mahalanobis distance indicates that the populations are more cleanly separated giving better earthquake/explosion discrimination. In order to avoid "cherry picking" the data, we have included the Hellum-1 explosion and the anomalous earthquake labeled events near the open-pit mines. As a reference point with the raw Pn/Sn amplitude ratios we find a Δ^2 of 0.28 for the 2-4 Hz band and Δ^2 of 1.00 for the 4-6 Hz band. In order to estimate a misclassification rate, we can translate a Mahalanobis distance value into an equiprobable point (EP), which is the point where the rate of earthquakes misclassified as explosions matches the rate of explosions that are misclassified as earthquakes, according to the formula:

$$EP = \Phi(-\frac{\Delta}{2}) \quad (4)$$

where Φ is the normal cumulative probability distribution. This results in equiprobable points of 39.6% for the 2-4 Hz band and 30.9% for the 4-6 Hz band. For the 1-D corrections, we find a Δ^2 of 2.46 for the 2-4 Hz band and Δ^2 of 4.50 for the 4-6 Hz band giving us equiprobable points of 21.6% and 14.4% for 2-4 Hz and 4-6 Hz bands, respectively. After applying the 2-D corrections from the attenuation model, we find Δ^2 of 10.06 and 9.35 for the two bands giving us equiprobable points of 5.6% and 6.3%. A summary of these results is provided in **Figure 6**. It appears, then, that the lateral attenuation corrections provide a larger improvement at lower frequencies. This is probably due to the better attenuation model in the lower frequency band, but potentially also due to more consistent and predictable amplitude variations at these frequencies. The use of reliable discriminants at lower frequencies should allow us to examine smaller, distant events that have lower signal-to-noise at higher frequencies.

Discussion

Two sets of outliers stand out in our Pn/Sn results, using both 1-D and 2-D path corrections. The first is the set of two presumed earthquake events just south of BRVK, at about the same epicentral distance as STS, which both classify as explosion-like. These events are at the location of a known large open-pit mine (Kevin Mackey, personal communication) and may not be natural earthquakes. While all of the presumed earthquakes in this study come from multiple catalogs where they are labeled as either earthquakes or unknown (and not explosions), it is possible that a few other presumed earthquakes in our dataset, particularly smaller events away from the seismically active areas to the south, might be unidentified mine-related events.

The second outlier is the Hellum-1 PNE, which comes out as earthquake-like at 2-4 and 4-6 Hz. According to Sultanov et al. (1999), Hellum-1 is a 3.2 kton explosion in limestone that is overburied at over 2.0 km (see **Table 1**). Examination of the waveforms shows a very strong Sn shear-wave signal from this nuclear explosion. One possible explanation would be if the path were very anomalous, and the path corrections we are using are invalid. Murphy et al. (2001) noted significant differences between PNE waveforms to the north and those to the northwest of BRVK and Bottone et al. (2001) noted some PNE 6-8 Hz P/S ratios were small in the region. However, this seems unlikely to be the cause of the Hellum-1 low P/S values observed here since we have four earthquakes nearby in the Ural Mountains and another northwest of Hellum-1, each of which have clear high frequency Pn and Sn phases constraining the path correction to BRVK reasonably well.

A second and more interesting possible explanation for the low Hellum-1 PNE P/S value might be related to its relatively small size and great depth. It is known that the explosion P-wave corner frequency depends upon depth, as described in the widely used model of Mueller and Murphy (1971). Fisk (2006, 2007) has postulated that explosion P/S values can be modeled using the Mueller-Murphy P-wave model where the S-wave are calculated by scaling the S-wave corner frequency by the ratio of the S to P-wave

velocity. Taylor (2009) has proposed that this S-wave corner frequency effect might be due to rock damage from the explosion and that it might persist even for very overburied events. In **Figure 7**, we show that using this explosion model predicts that the P/S value for Hellum-1 is expected to be much lower at 2-4 and 4-6 Hz than the other PNEs measured here.

However, if this model is correct, then some of the small explosions observed at the Semipalatinsk Test Site might also be expected to have similarly small P/S values, which is not observed. For example, the smallest Semipalatinsk explosions we have measured have m_b values near 3.7, which using the Murphy (1996) magnitude-yield formula of m_b=0.75 log(W)+4.45 (where W is yield in ktons), and would imply a yield of about ~0.1 kt (Khalturin et al., 2001). There is only very limited published information about the depth of STS nuclear tests, and based on that Israelsson (1994) estimates a very rough relationship of DOB=90$(W)^{1/3}$ m. This implies a depth of burial of about 40 m for a 0.1 kt and a depth of about 500 m for 150 kt. There are reasons to think that some of the small tests might be deeper than this relationship implies, for example, due to some of them occurring in tunnels with variable overburden (e.g. Khalturin et al., 2001). In **Figure 7** we show the explosion model P/S ratios for Semipalatinsk from 150 to 0.1 kt at a range of depths (assumed for our purposes to be in granite). If some of the small Semipalatinsk explosions were buried at depths of about 200 m, we would expect them to be outliers at 2-4 and 4-6 Hz as well. Given that the Hellum-1 PNE is the only significant explosion outlier, it would imply that if this model of P/S ratios is correct, the smallest explosions at Semipalatinsk are not significantly overburied. The physical mechanisms that generate explosion S-waves and our ability to model their P/S values for arbitrary depths and geologies remains an area of research.

As an example of the effects of emplacement, **Figure 8** shows a close-up of STS, where we can see the separation of explosions into several locations at Balapan, Degelan, and Murzhik. Events at all of these locations have effectively the same propagation path to BRVK, so variations will solely be due to source effects. We find several interesting things. First, the variation in the discriminant values from STS is only slightly lower than the variations from the distributed earthquakes which, besides unmodeled propagation effects, can also have additional variations from depth and radiation pattern. This means that, in the absence of large numbers of explosions, using the variation in the earthquake population would be a valid, conservative estimate. Secondly, we find significant variations among the locations, with events at Balapan having lower P/S ratios than events at Degelan and Murzhik. The regions differ from each other in terms of both geology and emplacement conditions. In Degelen, the mountain is a pluton and tests were carried out in tunnels and conducted in granite or porphyry. It seems possible that the tunnel tests might have a larger range in terms of scaled depth of burial. In contrast, at Balapan and Murzhik, the explosions were carried out in shafts. At Balapan, the rocks are generally tuffs or clastic rocks like conglomerate, sandstone, aleurolite, siltstones, and shales, while tests at Murzhik were carried out in clastic rock (Khalturin et al., 2001).

Conclusions

Using a combination of events from the historic Deglitched Borovoye Archive Dataset and more recent events from the modern instrument, we find that high-frequency P/S amplitudes can be used to reliably identify earthquakes and explosions in Central Asia. There is good discrimination between earthquakes and explosions both at the STS and for PNEs located throughout the region. More generally, we conclude that seismic discrimination is applicable over broad regions as long as propagation effects are properly accounted for. Applying 1-D and 2-D corrections markedly improves the performance of high-frequency P/S discriminants. Attenuation models that can account for the observed variations in amplitudes can further enhance our ability to identify events as earthquake or explosions, particularly in complex regions with stronger lateral variations than the region considered here. Accounting for lateral attenuation variations can also improve the discriminant at lower frequencies where more events and smaller events can be observed. Finally we note that using multiple frequency bands, including those over 6 Hz may provide the best means identify the full range of possible explosions including small and/or overburied events such as Hellum-1.

Acknowledgements

This work would not be possible without the tireless efforts of researchers at the Lamont-Doherty Earth Observatory and Los Alamos National Laboratory for compiling, deglitching and determining the instrument responses for thirty years of Borovoye data. We thank Paul Richards for providing boundaries of the Semipalatinsk Test Site (http://www.ldeo.columbia.edu/~richards/Semi.boundaries.html). We thank Terri Hauk and Stan Ruppert for maintaining the LLNL Seismic Research Database, Eric Matzel for making many of the amplitude measurements used in this study, and Alan Sicherman for his assistance with statistical analysis. We also thank Doug Dodge and Mike Ganzberger for the Regional Bodywave Amplitude Processor (RBAP), the tool used to make our amplitude measurements. This work was performed under the auspices of the U.S. Department of Energy by Lawrence Livermore National Laboratory under contract DE-AC52-07NA27344. This is LLNL contribution LLNL-JRNL-******.

References

Baker, D., W.-Y. Kim, H. Patton, G. Randall, and P. Richards (2009). Improvements to a major digital archive of seismic waveforms from nuclear explosions: The Borovoye seismogram archive, in Proceedings of the 2009 Monitoring Research Review: Ground-Based Nuclear Explosion Monitoring Technologies, LA-UR-09-05276, 12-21.

Bottone, S., M.D. Fisk, and G.D. McCartor (2001). Regional seismic event characterization using Bayesian calibration, Mission Research Corporation report, MRC-R-1621, 87 pp.

Bottone, S., M.D. Fisk, and G.D. McCartor (2002). Regional seismic event characterization using a Bayesian formulation of simple kriging, Bull. Seism. Soc. Amer., 92, 2277-2296.

Fisk, M.D. (2006). Source spectral modeling of regional P/S discriminants at nuclear test sites in China and the former Soviet Union, Bull. Seism. Soc. Amer., 96, 2348-2367.

Fisk, M.D. (2007). Corner frequency scaling of regional seismic phases for underground nuclear explosions at the Nevada Test Site, Bull. Seism. Soc. Amer., 97, 977-988.

Hartse, H., S.R. Taylor, W.S. Phillips, and G.E. Randall (1997). A preliminary study of regional seismic discrimination in Central Asia with an emphasis on Western China, Bull. Seism. Soc. Am. 87, 551-568.

Hartse, H.E., R.A. Flores, and P.A. Johnson (1998). Correcting regional seismic discriminants for path effects in Western China, Bull. Seism. Soc. Amer., 88, 596-608.

Israelsson, H. (1994). Analysis of historical seismograms – root mean square Lg magnitudes, yields, and depths of explosions at the Semipalatinsk Test Range, Geophys. J. Int., 117, 591-609.

Khalturin, V.I., T.G. Rautian, and P.G. Richards (2001). A study of small magnitude seismic events duing 1961-1989 on and near the Semipalatinsk Test Site, Kazakhstan, Pure Appl. Geophys., 158, 143-171, DOI: 10.1007/PL00001153.

Kim, W.-Y. and G. Ekstrom (1996). Instrument responses of digital seismographs at Borovoye, Kazakhstan, by inversion of transient calibration pulses, Bull. Seism. Soc. Amer., 191-203.

Kim. W.-Y., V. Aharonian, A.L. Lerner-Lam, and P.G. Richards (1997). Discrimination of earthquakes and explosions in southern Russia using regional high frequency three-component data from the IRIS/JSP Caucasus network, Bull. Seism. Soc. Amer., 87, 569-588.

Kim, W.-Y., P.G. Richards, V. Adushkin, and V. Ovtchinnikov (2001). Borovoye digital archive for underground nuclear tests during 1966-1996, Lamont-Doherty Earth Observatory Report, www.ldeo.columbia.edu/Monitoring/Data/Brv_arch_ex/brv_text_table.pdf

Mueller, R.A. and J.R. Murphy (1971). Seismic characteristics of underground nuclear detonations: Part I. Seismic scaling law of underground detonations, Bull. Seism. Soc. Amer., 61, 1675-1692.

Murphy, J.R. (1996). Types of seismic events and their source descriptions, in Monitoring a Comprehensive Test Ban Treaty, E.S. Husebye and A.M Dainty, eds., 225-245.

Murphy, J.R., I.O. Kitov, B.W. Barker, and D.D. Sultanov (2001). Seismic source characeristics of Soviet peaceful nuclear explosions, Pure Appl. Geophys., 158, 2077-2101.

Pasyanos, M.E. and W.R. Walter (2009). Improvements to regional explosion identification using attenuation models of the lithosphere, Geophys. Res. Lett., L14304, doi:10.1029/2009GL038505.

Pasyanos, M.E., W.R. Walter, and E.M. Matzel (2009). A simultaneous multi-phase approach to determine P-wave and S-wave attenuation of the crust and upper mantle, Bull. Seism. Soc. Amer., 99, DOI: 10.1785/0120090061.

Phillips, W.S., X. Yang, G.E. Randall, H.E. Hartse, and R.J. Stead (2009). Regional phase attenuation tomography for central and eastern Asia in Proceedings of the 2009 Monitoring Research Review: Ground-based Nuclear Explosion Monitoring Technologies, LA-UR-09-05276, 536-546.

Richards, P.G., W.-Y. Kim, and G. Ekstrom (1992). Borovoye Geophysical Observatory, Kazakhstan, EOS Trans. Am. Geophys. Union, 73, 201-202, doi:10.1029/91EO00161.

Rodgers, A.J. and W.R. Walter (2002). Seismic discrimination of the May 11, 1998 Indian nuclear test with short-period regional data from station NIL (Nilore, Pakistan), Pure Appl. Geophys., 159, 679-700, DOI: 10.1007/s00024-002-8654-6.

Sultanov, D.D., J.R. Murphy and Kh.D. Rubinstein (1999). A seismic source summary for Soviet peaceful nuclear explosions, Bull. Seism. Soc. Am. 89, 640–647.

Taylor, S. (1996). Analysis of high-frequency Pg/Lg ratios from NTS explosions and western U.S. earthquakes, Bull. Seism. Soc. Amer., 86, 1042-1053.

Taylor, S., A. Velasco, H. Hartse, W.S. Phillips, W.R. Walter, and A. Rodgers (2002). Amplitude corrections for regional discrimination, Pure. App. Geophys., 159, 623-650.

Taylor, S.R. (2009). Can the Fisk conjecture be explained by rock damage around explosions? Bull. Seism. Soc. Amer., 99, 2552-2555, doi:10.1785/0120080332.

Walter, W.R. and S.R. Taylor (2001). A revised magnitude and distance amplitude correction (MDAC2) procedure for regional seismic discriminants: theory and testing at NTS, LLNL UCRL-ID-146882, http://www.llnl.gov/tid/lof/documents/pdf/240563.pdf

Walter, W.R., K. Mayeda, and H.J. Patton (1995). Phase and spectral ratio discrimination between NTS earthquakes and explosions Part 1: Empirical observations, Bull. Seism. Soc. Am., 85, 1050-1067.

Walter, W.R., E. Matzel, M.E. Pasyanos, D.B. Harris, R. Gok, and S.R. Ford (2007). Empirical observations of earthquake and explosion discrimination using P/S ratios and implications for the sources of explosion S-waves, in Proceedings of the 29th Monitoring Research Review, LA-UR-07-5613, 684-693.

Figure captions

Figure 1. Maps of the study area in Central Asia. a) Map showing topography and tectonic provinces. Location of Borovoye station is indicated by triangle. STS indicates the Semipalatinsk Test Site. b) Path map of amplitude measurements for Pn at 2-4 Hz. Events are indicated as circles, and stations as triangles. c) Map of the upper mantle attenuation (Qp) at 2-4 Hz from multi-phase amplitude tomography (Pasyanos et al., 2009). d) Map of path-average Pn attenuation to station BRVK from map points.

Figure 2. Raw discrimination results for Pn/Sn discriminant. a) Map view of discriminant at 2-4 Hz; b) Map view of discriminant at 4-6 Hz; c) Discriminant as a function of distance at 2-4 Hz; d) Discriminant as a function of distance at 4-6 Hz. In all plots, explosions are indicated by stars, and presumed earthquakes as circles.

Figure 3. Discrimination results for Pn/Sn discriminant corrected for 1-D propagation effects. a) Map view of discriminant at 2-4 Hz; b) Map view of discriminant at 4-6 Hz; c) Discriminant as a function of distance at 2-4 Hz; d) Discriminant as a function of distance at 4-6 Hz. In all plots, explosions are indicated by stars, and presumed earthquakes as circles.

Figure 4. Discrimination results for Pn/Sn discriminant corrected for lateral propagation effects. a) Map view of discriminant at 2-4 Hz; b) Map view of discriminant at 4-6 Hz; c) Discriminant as a function of distance at 2-4 Hz; d) Discriminant as a function of distance at 4-6 Hz. In all plots, explosions are indicated by stars, and presumed earthquakes as circles.

Figure 5. Discrimination results for Pn/Sn discriminant corrected for lateral propagation effects. a) Discriminant as a function of magnitude at 2-4 Hz; b) Discriminant as a function of magnitude at 4-6 Hz. In all plots, explosions are indicated by stars, and presumed earthquakes as circles.

Figure 6. A summary of the discrimination results in this study showing the Mahalanobis distance Δ^2 (left axis) and equiprobable point (right axis) at 1-2, 2-4, 4-6, and 6-8 Hz for raw amplitude ratios (red), and 1-D (yellow) and 2-D (green) path corrected amplitude ratios. Numbers of earthquakes and explosions observed in that frequency band are provided at the top of the figure.

Figure 7. Model of explosion P/S values using the Mueller-Murphy (1971) P-wave model and the Fisk (2006, 2007) conjecture S-wave model for the PNEs and Semipalatinsk explosions. As the depths of the STS explosions are not known, a range of possible

values is shown. Heavier shading indicates the region covered by the Israelsson (1994) depth of burial scaling, while the lighter shading show values when the smaller events are overburied.

Figure 8. Discrimination results for Pn/Sn discriminant focused on the Semipalatinsk Test Site. a) Map view of discriminant at 2-4 Hz; b) Map view of discriminant at 4-6 Hz.

Table 1. Peaceful Nuclear Explosions recorded at regional distances at Borovoye. All values in the table are from Sultanov et al. (1999).

PNE Name	Date (mm/dd/yyyy)	Location	Medium	Yield (kt)	Depth (m)
Meridian-1	8/23/1973	50.527º N 68.323º E	Sandstone/shale	6.3	395
Meridian-2	9/19/1973	45.758º N 67.825º E	Sandstone/shale	6.3	615
Hellum-1	9/2/1981	60.60º N 55.70º E	Limestone	3.2	2088
Batholith-2	10/3/1987	47.60º N 56.20º E	Salt	8.5	1002

Figure 1

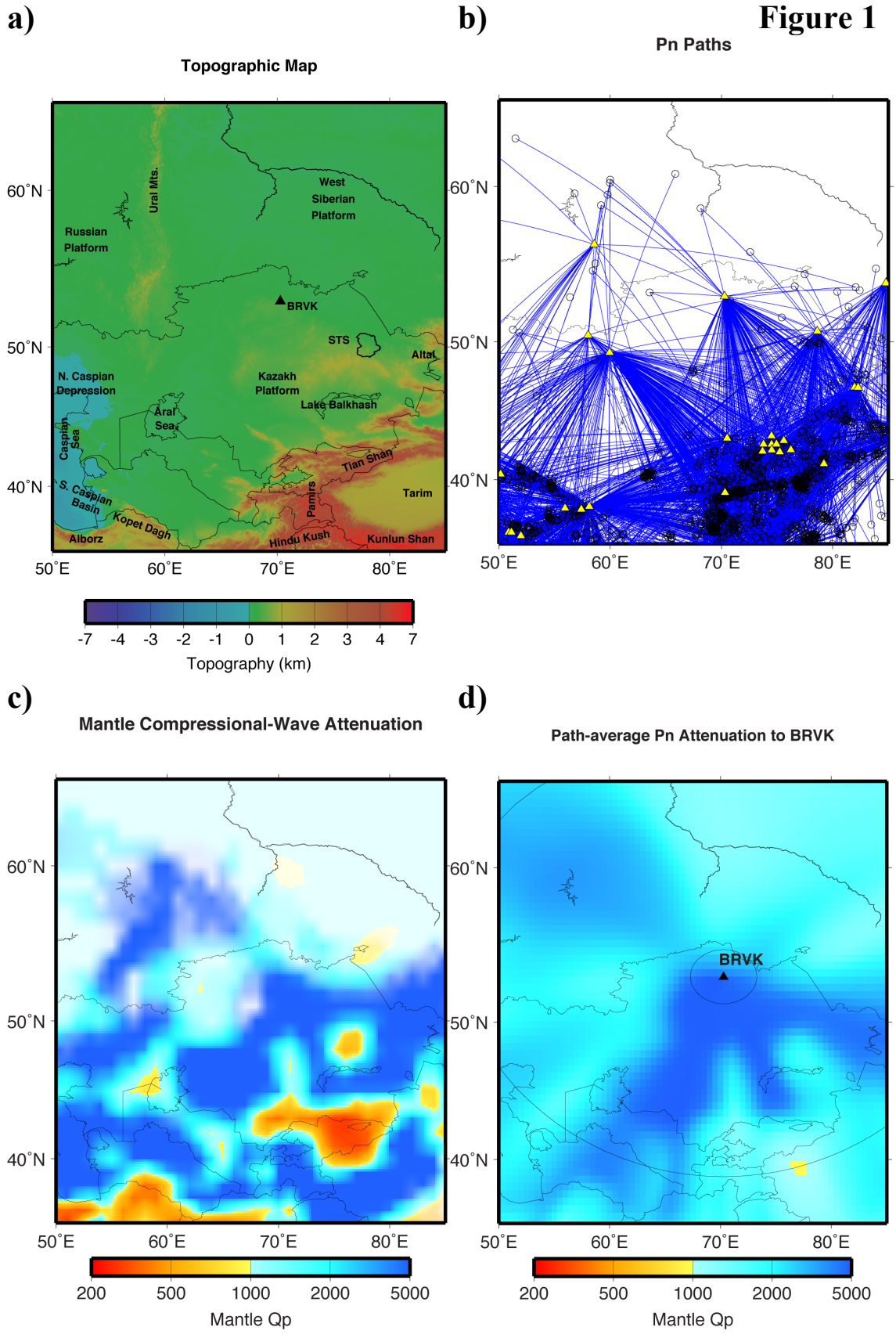
a)
Topographic Map
Ural Mts.
West Siberian Platform
Russian Platform
BRVK
STS
Altai
N. Caspian Depression
Kazakh Platform
Lake Balkhash
Aral Sea
Caspian Sea
Tian Shan
Tarim
S. Caspian Basin
Kopet Dagh
Pamirs
Alborz
Hindu Kush
Kunlun Shan
60°N
50°N
40°N
50°E
60°E
70°E
80°E
-7 -4 -3 -2 -1 0 1 2 3 4 7
Topography (km)
b)
Pn Paths
c)
Mantle Compressional-Wave Attenuation
200 500 1000 2000 5000
Mantle Qp
d)
Path-average Pn Attenuation to BRVK
BRVK
200 500 1000 2000 5000
Mantle Qp

Figure 2

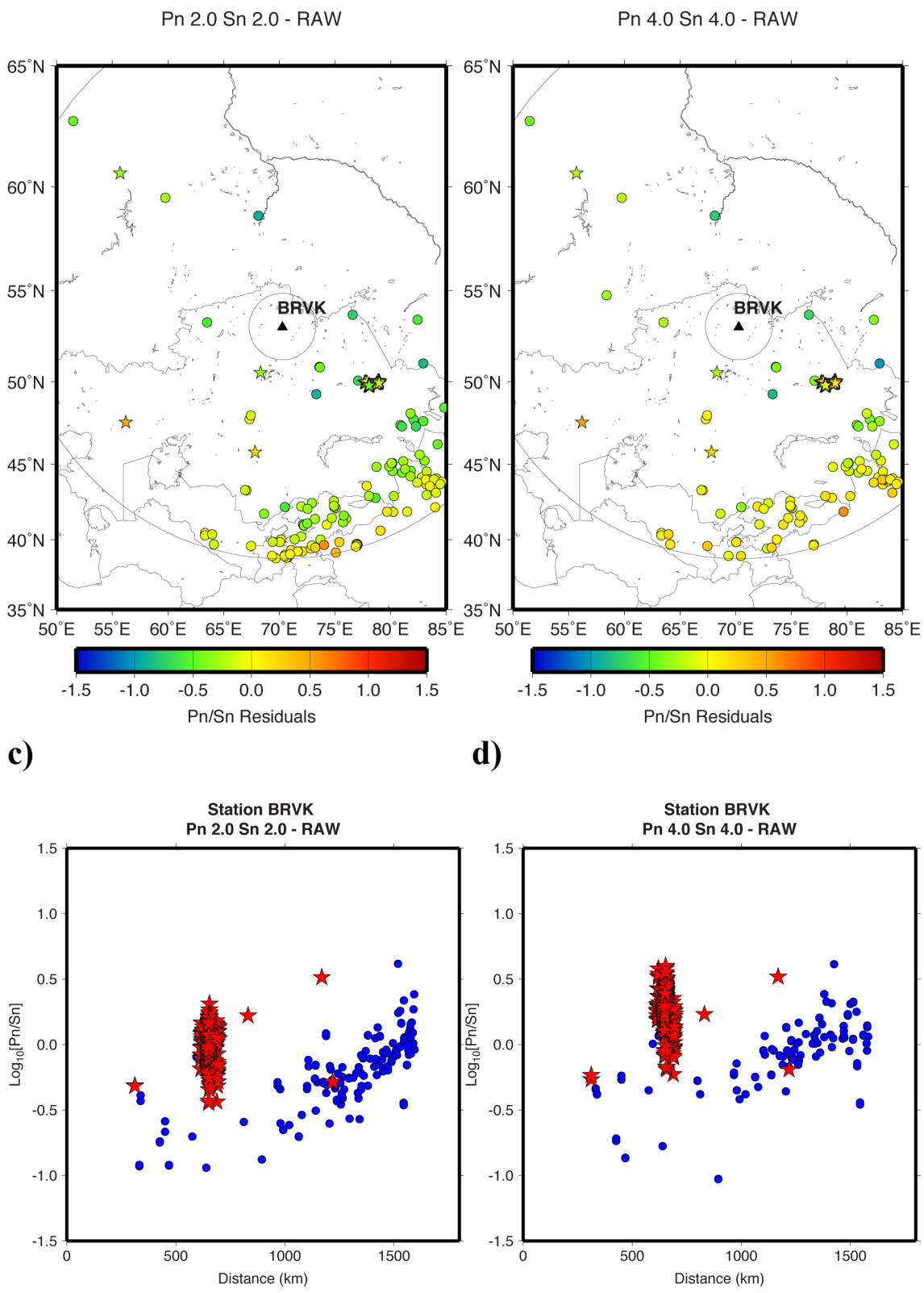
a)
b)
Pn 2.0 Sn 2.0 - RAW
Pn 4.0 Sn 4.0 - RAW
BRVK
65°N
60°N
55°N
50°N
45°N
40°N
35°N
50°E
55°E
60°E
65°E
70°E
75°E
80°E
85°E
-1.5
-1.0
-0.5
0.0
0.5
1.0
1.5
Pn/Sn Residuals
c)
d)
Station BRVK
Pn 2.0 Sn 2.0 - RAW
Pn 4.0 Sn 4.0 - RAW
Log10[Pn/Sn]
Distance (km)
0
500
1000
1500

a) **b)** **Figure 3**

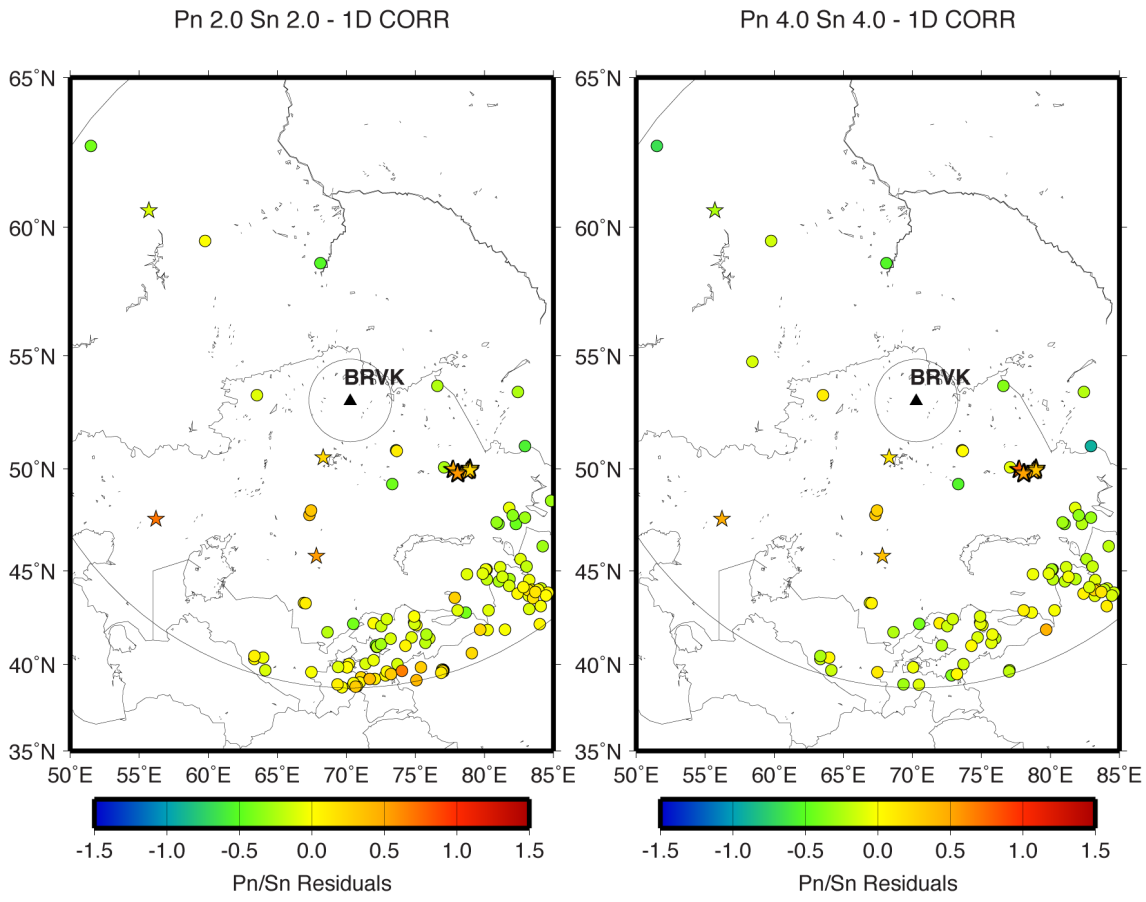

c) **d)**

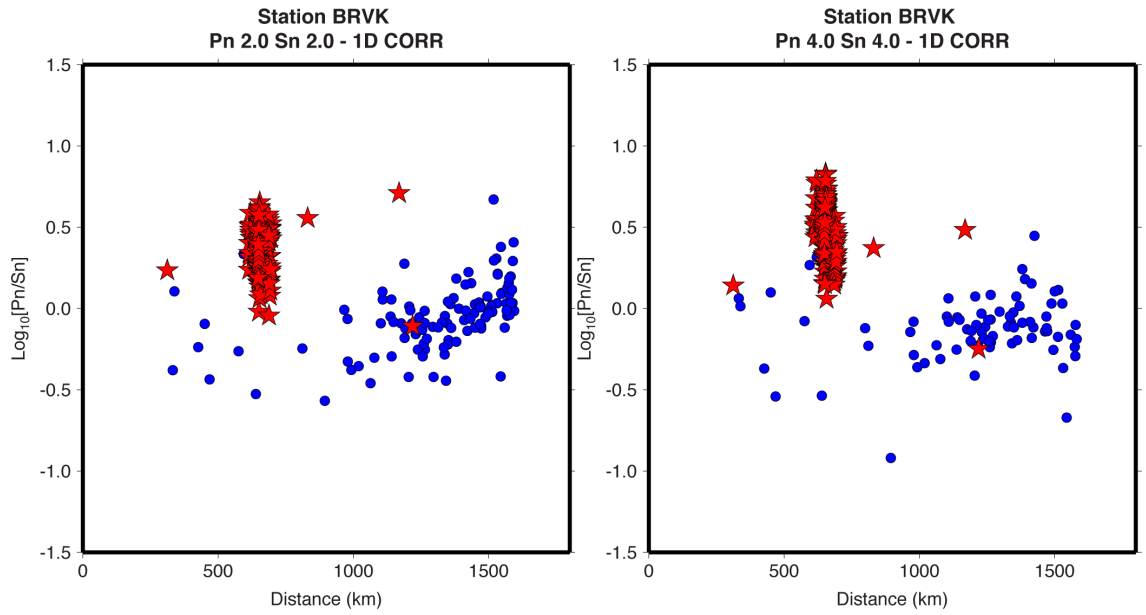

a) **b)** **Figure 4**

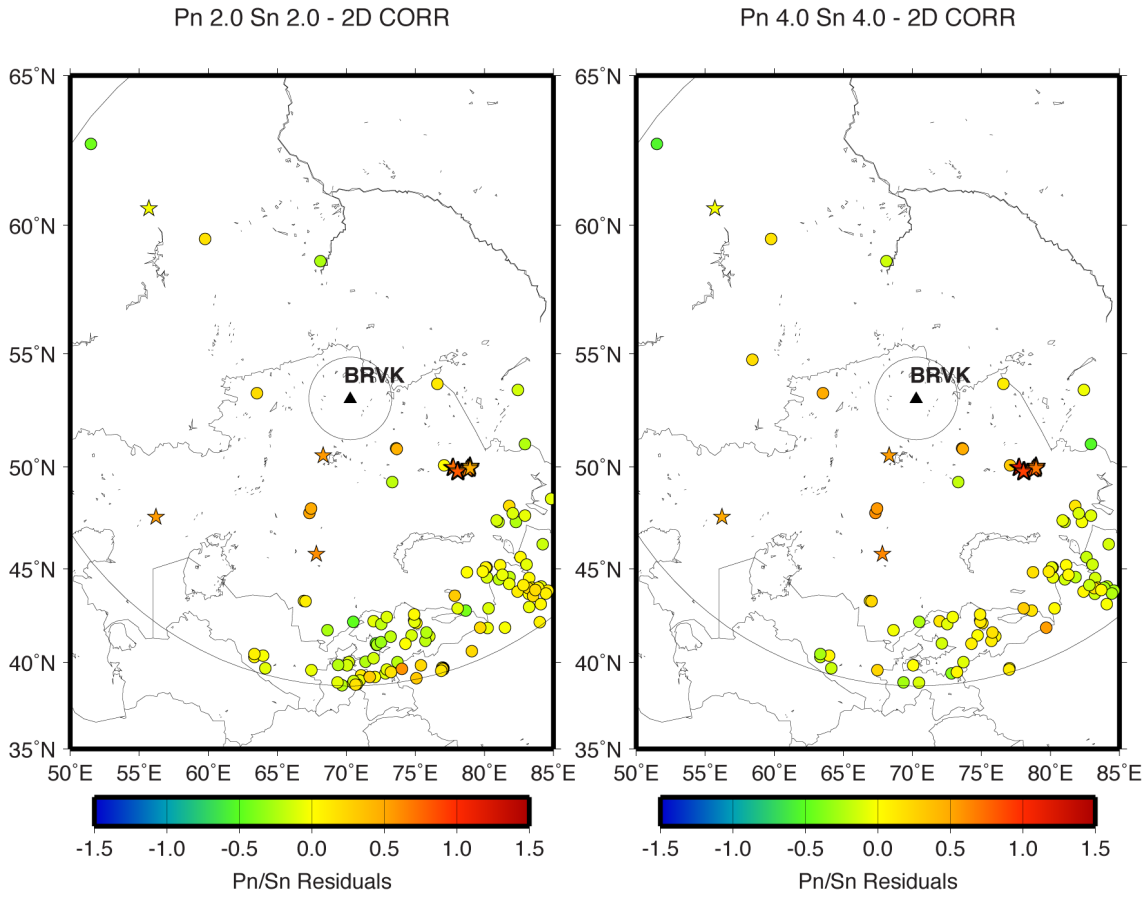

c) **d)**

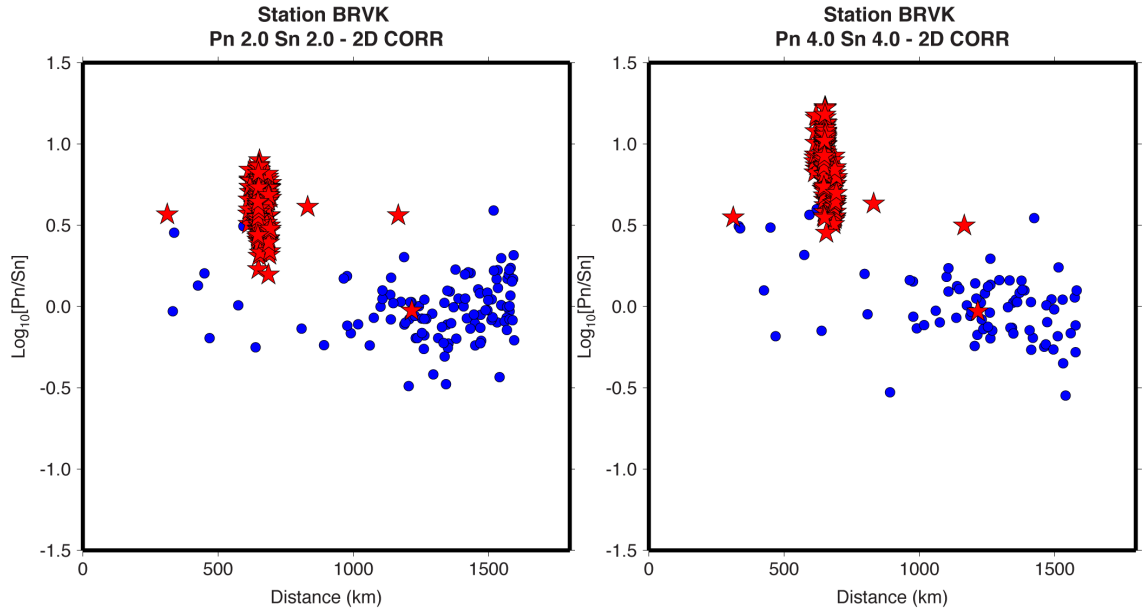

a) **b)** **Figure 5**

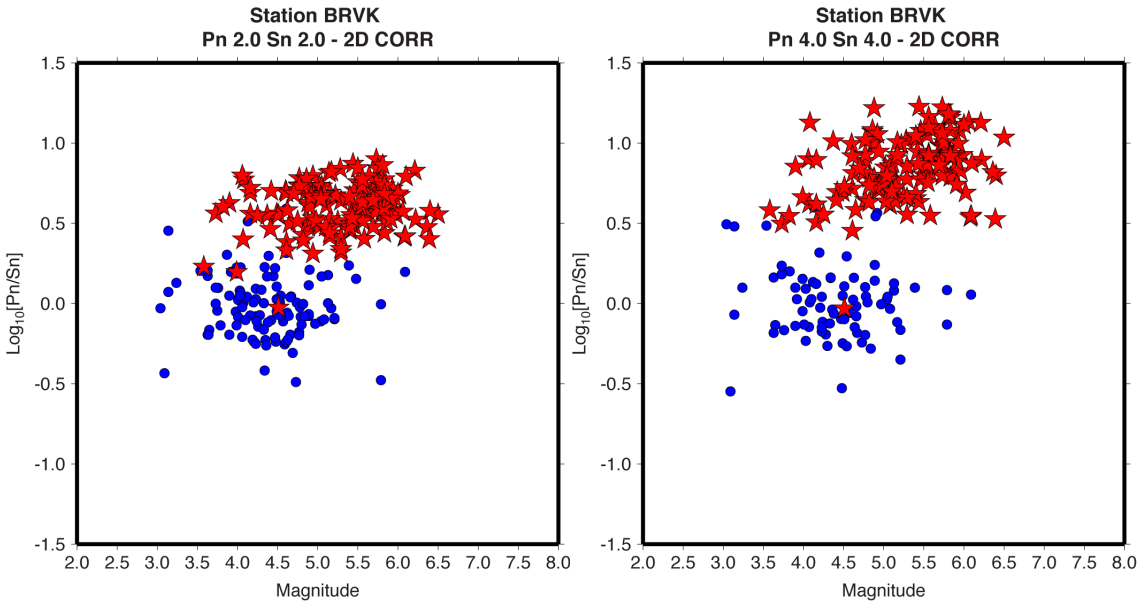
Station BRVK
Pn 2.0 Sn 2.0 - 2D CORR
Log10[Pn/Sn]
Magnitude
Station BRVK
Pn 4.0 Sn 4.0 - 2D CORR
Log10[Pn/Sn]
Magnitude

Figure 6

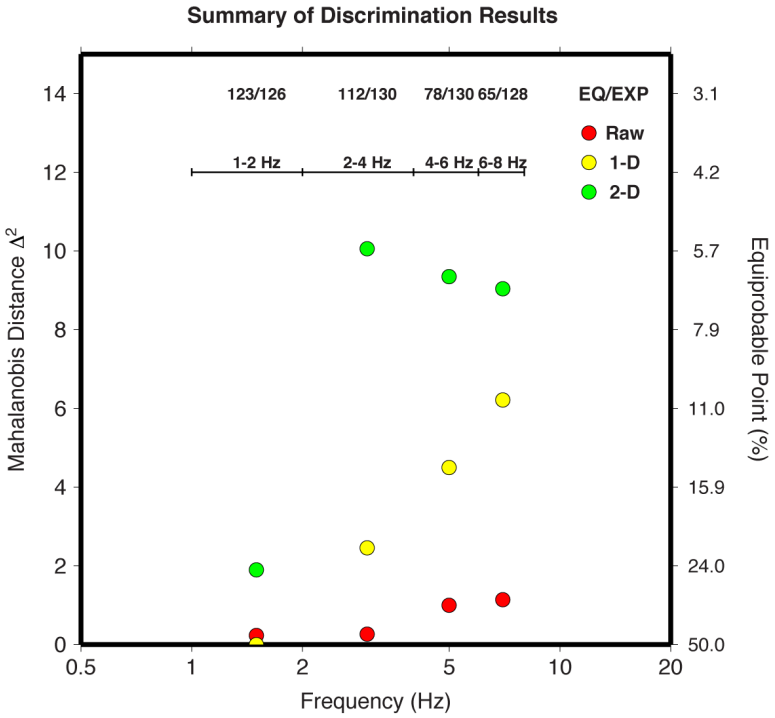
Summary of Discrimination Results
123/126
112/130
78/130
65/128
EQ/EXP
Raw
1-D
2-D
1-2 Hz
2-4 Hz
4-6 Hz
6-8 Hz
Mahalanobis Distance Δ²
Equiprobable Point (%)
Frequency (Hz)
0
2
4
6
8
10
12
14
0.5
1
2
5
10
20
3.1
4.2
5.7
7.9
11.0
15.9
24.0
50.0

Figure 7

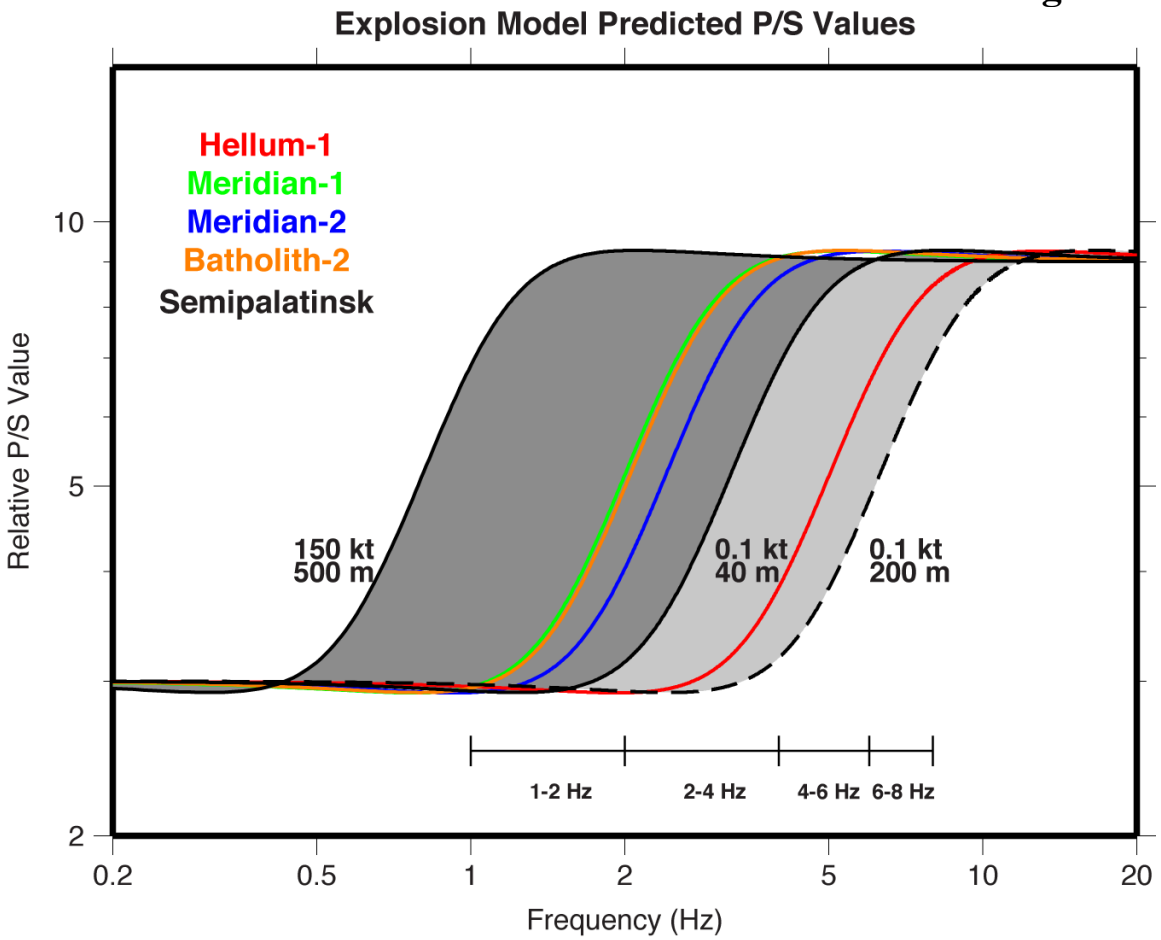
Explosion Model Predicted P/S Values
Hellum-1
Meridian-1
Meridian-2
Batholith-2
Semipalatinsk
150 kt
500 m
0.1 kt
40 m
0.1 kt
200 m
1-2 Hz
2-4 Hz
4-6 Hz
6-8 Hz
Relative P/S Value
10
5
2
0.2
0.5
1
2
5
10
20
Frequency (Hz)

a) **b)** **Figure 8**

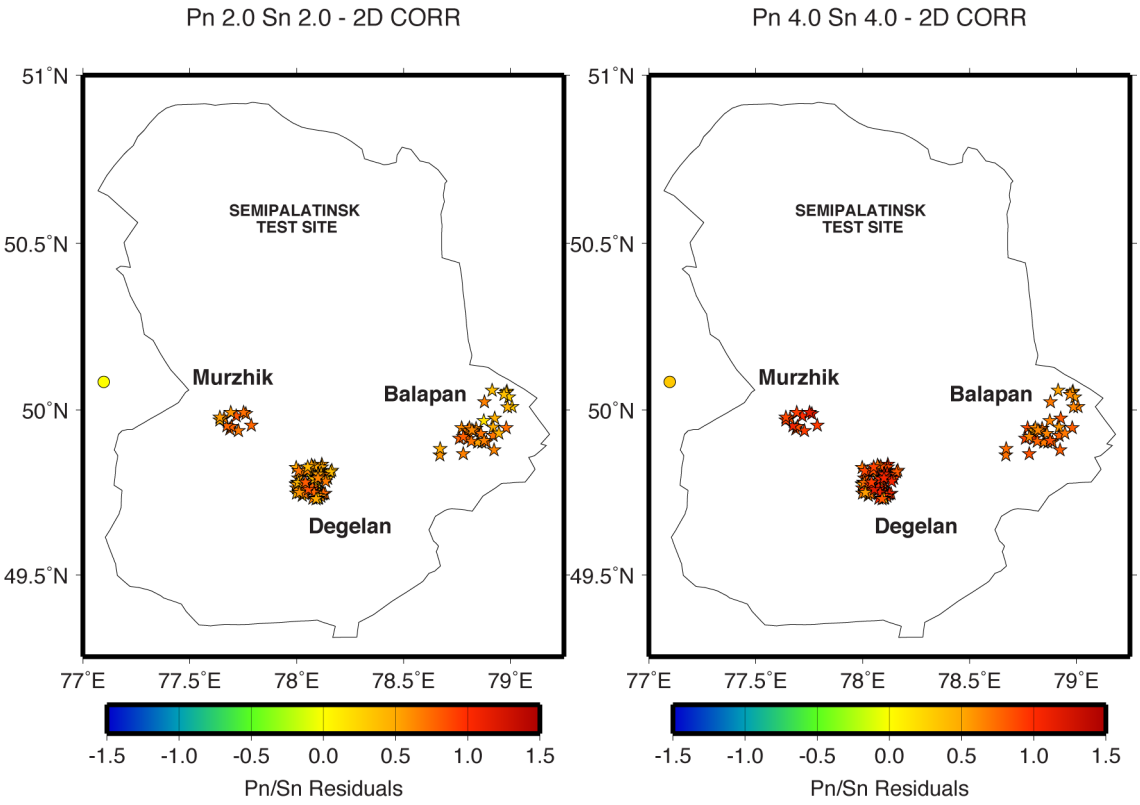
Pn 2.0 Sn 2.0 - 2D CORR
Pn 4.0 Sn 4.0 - 2D CORR
SEMIPALATINSK
TEST SITE
Murzhik
Balapan
Degelan
51°N
50.5°N
50°N
49.5°N
77°E
77.5°E
78°E
78.5°E
79°E
-1.5
-1.0
-0.5
0.0
0.5
1.0
1.5
Pn/Sn Residuals